Geophys. J. Int. (2001) **145,** 721–730

First-order reversal curve diagrams and thermal relaxation effects in magnetic particles

Christopher R. Pike,[1] Andrew P. Roberts[2] and Kenneth L. Verosub[1]

[1] *Department of Geology, University of California, Davis,* CA 95616, *USA*
[2] *School of Ocean and Earth Science, University of Southampton, Southampton Oceanography Centre, European Way, Southampton,* SO14 3ZH, *UK.*
E-mail: andrew.p.roberts@soc.soton.ac.uk

Accepted 2001 January 8. Received 2001 January 8; in original form 2000 July 3

SUMMARY

We have recently developed a technique for characterizing the magnetic components within natural particle assemblages. This technique is based on the transformation of magnetization data from first-order reversal curves (FORCs) into contour plots of a 2-D distribution function (FORC diagrams). FORC diagrams are useful for obtaining information about switching fields and interactions in magnetic particle systems. Here, we examine experimental data and a theoretical model in order to provide a rigorous framework for interpreting FORC diagrams for samples that contain superparamagnetic particles. We have found four distinct manifestations of thermal relaxation on FORC diagrams. First, thermal relaxation will shift the FORC distribution to lower coercivities. Second, at intermediate temperatures, thermal relaxation can generate a secondary peak about the origin of a FORC diagram. This secondary peak indicates that part of a single-domain particle assemblage has become superparamagnetic. At high enough temperatures, the primary peak of the FORC distribution will be located about the origin of a FORC diagram. Third, thermal relaxation can produce a small, but systematic, upward shift of a FORC distribution. Fourth, thermal relaxation will produce contours that lie near and parallel to the vertical axis in the lower quadrant of a FORC diagram. These manifestations make FORC diagrams a powerful tool for studying the effects of thermal relaxation (superparamagnetism) in bulk natural samples, particularly when the samples contain mixed magnetic particle assemblages.

Key words: environmental magnetism, FORC diagram, single domain, superparamagnetism, thermal relaxation.

INTRODUCTION

Superparamagnetic (SP) behaviour occurs in single-domain particles below a critical size, where thermal energy becomes large enough to switch spontaneously the magnetic moments of the particles on a laboratory timescale (Néel 1949). SP behaviour is commonly observed in rocks and sediments. These fine particles have been the focus of much recent attention because of their importance in environmental and rock magnetic studies (e.g. Forster *et al.* 1994; Dearing *et al.* 1996; Eyre 1997; Moskowitz *et al.* 1997; Worm 1998, 1999; Worm & Jackson 1999).

We have recently developed a technique for characterizing the magnetic components within mixed natural particle assemblages (Pike *et al.* 1999; Roberts *et al.* 2000). The method is based on the transformation of magnetization data from first-order reversal curves (FORCs) into contour plots (FORC diagrams) of a 2-D distribution function. FORC diagrams have been used to study magnetic interactions in magnetic recording media (Pike *et al.* 1999), vortex nucleation and annihilation in cobalt dots (Pike & Fernandez 1999), and a range of geological samples encountered in environmental magnetic studies (Roberts *et al.* 2000).

The measurement and calculation of FORC diagrams have been described in more detail elsewhere (Pike *et al.* 1999; Roberts *et al.* 2000). In brief, a FORC diagram is calculated from a class of partial hysteresis curves known as first-order reversal curves or FORCs (see Mayergoyz 1986). As shown in Fig. 1(a), measurement of a FORC begins by saturating a sample in a large positive applied field. The field is decreased to a reversal field, H_a, and the FORC is defined as the magnetization curve that results when the applied field is increased from H_a back to saturation. The magnetization at the applied field, H_b, on the FORC with reversal point H_a is denoted by $M(H_a, H_b)$, where $H_b \geq H_a$. In a set of FORC measurements, the reversal fields must be evenly spaced, with field spacing FS; successive magnetization measurements on each FORC are

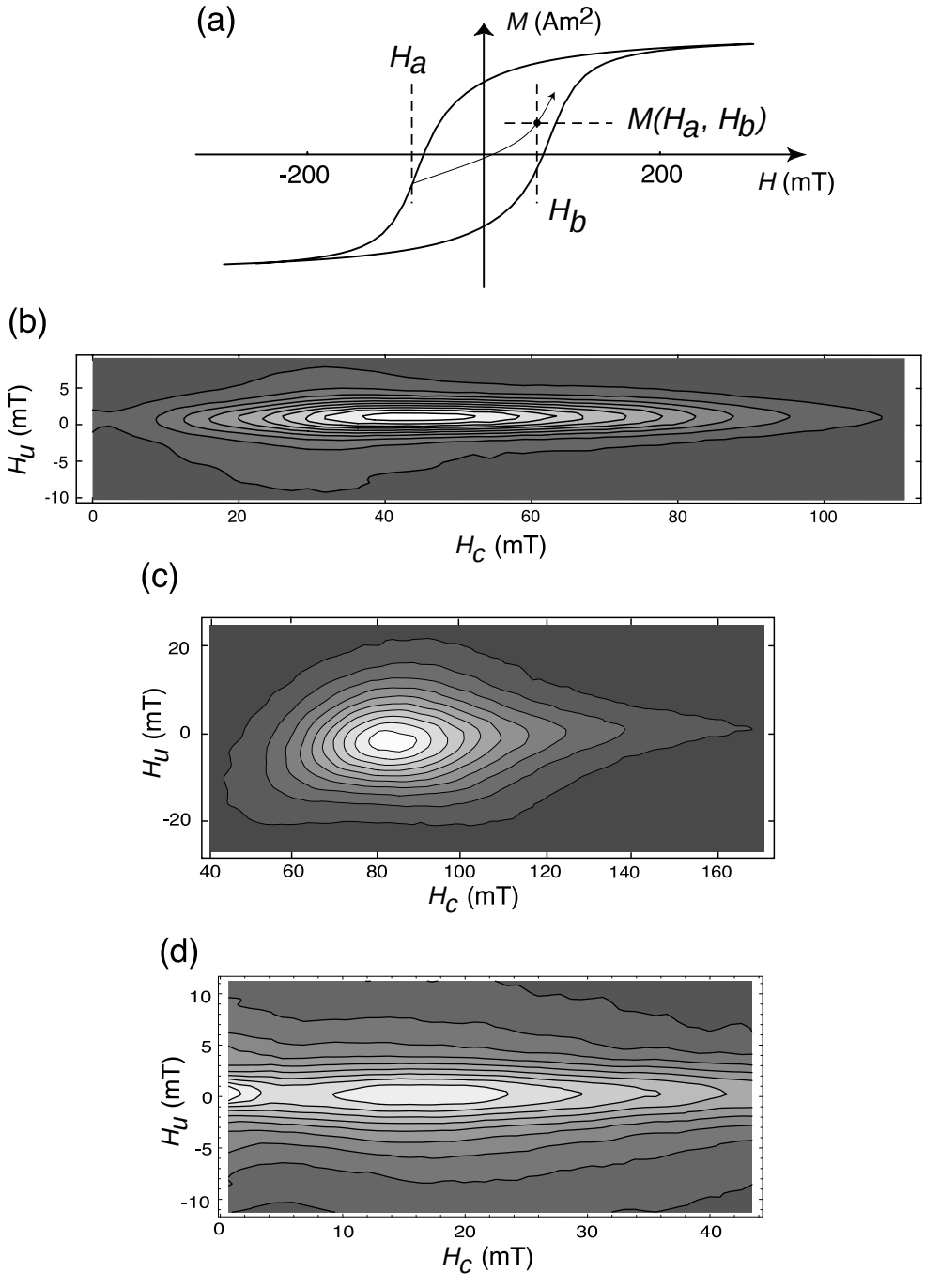

Figure 1. (a) Example of a major hysteresis loop with reversal point at H_a. The first-order reversal curve (FORC) is the curve that starts at H_a and proceeds back to positive saturation. The magnetization at any point H_b along the FORC is represented by $M(H_a, H_b)$. (b) FORC diagram for sample CS911 (see Worm 1998, 1999) containing non-interacting single-domain titanomagnetite particles (see Roberts *et al.* 2000). (c) FORC diagram for an Imation 2HD 1.44 MB magnetic floppy recording disk containing strongly interacting single-domain particles (see Pike *et al.* 1999). (d) High-resolution FORC diagram for sample BV1126 (see Roberts *et al.* 1996) from Pleistocene lake sediments. The sample contains non-interacting single-domain magnetite particles with a primary peak at $H_a \approx 18$ mT and a secondary peak near the origin of the FORC diagram due to thermal relaxation of part of the single-domain particle assemblage (see Roberts *et al.* 2000).

also made with this same field spacing. The same measurement time, t_m, is spent at each data point. A FORC distribution is defined as the mixed second derivative,

$$\rho(H_a, H_b) \equiv -\frac{\partial^2 M(H_a, H_b)}{\partial H_a \partial H_b}, \qquad (1)$$

which is well defined for $H_b > H_a$. When a FORC distribution is plotted, it is convenient to change coordinates from $\{H_a, H_b\}$ to $\{H_u = (H_a + H_b)/2,\ H_c = (H_b - H_a)/2\}$. A FORC diagram (Figs 1b–d) is a contour plot of a FORC distribution with H_u and H_c on the vertical and horizontal axes, respectively. A certain amount of numerical smoothing is always necessary

in the calculation of a FORC distribution from experimental data: the degree of smoothing is determined by a smoothing factor (*SF*). The FORC distribution for a non-interacting single-domain system (Fig. 1b), when thermal relaxation effects are negligible, has horizontally elongated contour loops, with little vertical spread. The H_c coordinate of the distribution peak corresponds to the median particle switching field. Magnetostatic interactions cause increased vertical spread (Fig. 1c) of the FORC distribution.

In our studies of natural samples, we have found that, in many instances, the FORC distribution has a secondary peak (Fig. 1d) about the origin of the FORC diagram (Roberts *et al.* 2000). We have attributed this secondary peak to the presence of SP particles resulting from thermal relaxation effects. At first, the presence of such a secondary peak was surprising because the magnetization of SP particles is entirely reversible and reduces to zero when the derivative is taken with respect to H_a in eq. (1). Thus, SP particles would not be expected to produce any manifestation on a FORC diagram. However, particles at or just below the SP threshold volume will behave in a quasi-reversible manner. That is, when the applied field switches direction there will be a small but detectable relaxation time as these particles overcome their energy barriers and switch direction. Consider two FORCs: an upper FORC with H_a just greater than zero, and a lower FORC with H_a just less than zero. At the reversal point of the lower FORC ($H_a<0$), some of these quasi-SP particles will have reversed (where these particles are not reversed on the upper curve). As the applied field is increased from H_a, the magnetization on the lower FORC will briefly lag behind the upper FORC due to the above-described relaxation effect. The small difference between these two FORCs will create a non-zero result when calculating the derivative with respect to H_a in eq. (1). The result is a contribution to a FORC distribution that is located at H_a, $H_b=0$ (i.e. at H_u, $H_c=0$). Hence, thermal relaxation effects involving material at or just below the SP threshold volume can explain the observation of a secondary peak about the origin of a FORC diagram.

In this paper, we undertake a more rigorous study of the manifestations of thermal relaxation on FORC diagrams for non-interacting single-domain particle systems. We compare experimental data with simulated FORC diagrams generated from a theoretical model of thermal relaxation in a non-interacting, uniaxially anisotropic single-domain particle system. FORC diagrams have considerable potential as a diagnostic tool for use in studying magnetic particle assemblages, particularly for identifying components in mixed magnetic assemblages where other techniques are often ambiguous. It is therefore important to provide a firm theoretical basis for the interpretation of features on FORC diagrams.

There are obvious similarities between a FORC diagram and a Preisach diagram (Preisach 1935). The similarities and differences between these two types of diagrams are discussed in greater detail elsewhere (Pike *et al.* 1999; Roberts *et al.* 2000). We prefer to use the term 'FORC diagram' to underscore several important distinctions between the two types of diagrams. Regardless, it is worth noting that there is little published experimental work on the effects of temperature and magnetic viscosity on Preisach diagrams for geological samples (see Mullins & Tite 1973; Dunlop *et al.* 1990). The manifestations of thermal relaxation that we have observed on FORC diagrams have not been reported before.

Samples

In this study, we present results for three samples that are affected by thermal relaxation. The first sample consists of 99.95 per cent pure synthetic anhydrous haematite (α-Fe_2O_3) powder, manufactured by Fisher Scientific (lot number 947483). The sample was mixed into a silicon grease matrix for measurement. The second sample is a haematite-rich Aptian red-bed sample from the south of France (90-VAU-42). The presence of SP particles is indicated by a value of 7 per cent for the frequency dependence of magnetic susceptibility. The possibility that significant proportions of SP particles can occur in haematite-rich sediments is consistent with what has been known for many years (e.g. Creer 1961; Collinson 1969). The third sample (CS914) is from the titanomagnetite-bearing Yucca Mountain ash flow tuff from southern Nevada (Schlinger *et al.* 1988; Eick & Schlinger 1990; Worm 1998, 1999; Worm & Jackson 1999). This sample has an exceptionally high value of 30 per cent for the frequency dependence of magnetic susceptibility (Worm 1998, 1999) which demonstrates that it is dominated by SP particles. The coercivity and remanence for sample CS914 are small and depend sensitively on the rate at which a hysteresis loop is scanned: the coercivity becomes vanishingly small when the scan rate is zero. These observations support the conclusions of Worm (1998, 1999) concerning the dominance of SP particles in sample CS914. We were unable to saturate magnetically the red-bed and synthetic haematite samples with our magnetometer (at maximum applied fields of 1.4 T). The measured hysteresis loops (Fig. 2) therefore do not give a valid coercive field or saturation remanence or saturation magnetization. We normalized these hysteresis loops so that they have a value of one and zero slope at the maximum applied field (Fig. 2). The red-bed sample yields a wasp-waisted hysteresis loop (Roberts *et al.* 1995; Tauxe *et al.* 1996) due to the combined effects of single-domain haematite (high coercivity), magnetite (relatively low coercivity) and SP particles (zero coercivity).

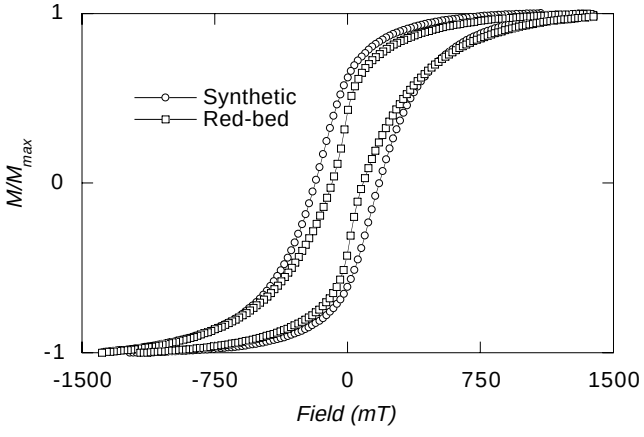

Figure 2. Major hysteresis loops for synthetic haematite and natural red-bed samples. The curves were normalized to unity and have zero slope at the maximum applied field. Note that the red-bed sample contains a mixture of single-domain haematite, single-domain magnetite and a significant superparamagnetic haematite component; a mixture of these components produces the wasp-waisted shape of the hysteresis loop.

EXPERIMENTAL RESULTS

FORC diagrams for the three studied samples are shown in Figs 3–5. The FORC diagram for the synthetic haematite sample (Fig. 3a) yields a peak at about $H_c = 150$ mT and highly elongated horizontal contours, which are characteristic of high coercivity, single-domain haematite particles with only weak interactions (*cf.* Fig. 1b). The fact that some of the contours meet the vertical axis indicates that the distribution has been shifted slightly to lower coercivities by thermal relaxation effects. The FORC distribution for sample 90-VAU-42 (Fig. 4a) also extends out to high coercivities. However, the distribution lies much further to the left than the distribution for the synthetic haematite sample (Fig. 3a), and the peak of the distribution no longer has closed single-domain contours but is centred about the origin of the FORC diagram. To observe the details of the FORC distribution for sample 90-VAU-42, we acquired a higher-resolution FORC diagram (with a finer field spacing), as shown in Fig. 4(b). The weak peak centred at $\sim$20 mT is due to the presence of non-interacting magnetite particles. The secondary peak located about the origin of the FORC diagram can be attributed to SP haematite particles (see below).

The FORC distribution for sample CS914 (Fig. 5) is shifted even closer to the origin than those for the previous two samples. This is an indication of a dominant SP content, which is in agreement with the findings of Worm (1998, 1999) and Worm & Jackson (1999). The nearly vertical contours that extend into the lower quadrant of the FORC diagrams are another striking feature of Figs 4 and 5. Having observed these nearly vertical contours, we re-examined the synthetic haematite sample with a higher-resolution FORC diagram in the lower half-plane (Fig. 3b). This diagram contains purely vertical lines. For the synthetic sample, this effect is slight and the value of the FORC distribution in the region of Fig. 3(b) is small compared to the values at the peak of the FORC distribution (Fig. 3a). These vertical lines therefore do not appear in the normal-resolution FORC diagram (Fig. 3a).

To help interpret the experimental results presented in Figs 3–5, we compare them with the FORC diagrams generated from a theoretical model of non-interacting, uniaxially anisotropic, single-domain particles, including thermal relaxation effects.

THEORETICAL MODEL

(i) Uniform H_k and V

Let us begin with a collection of particles with volume V, spontaneous magnetization M_s and anisotropy field H_k, where the uniaxial anisotropy axis is aligned with the z-axis of the particles. Let $n\uparrow$ denote the fraction of particles with moments in the 'up' direction (i.e. positive z), and let $n\downarrow$ denote the fraction of particles with moments in the 'down' direction (i.e. negative z). Let us define the dimensionless magnetization $M = n\uparrow - n\downarrow$, where $n\uparrow + n\downarrow = 1$. Let $\Delta E\uparrow\downarrow$ and $\Delta E\downarrow\uparrow$ denote the energy barriers to the transition of a particle moment from up to down and vice versa. In an applied field H (aligned with the z-axis), $\Delta E\uparrow\downarrow$ and $\Delta E\downarrow\uparrow$ can be written as (Pfeiffer &

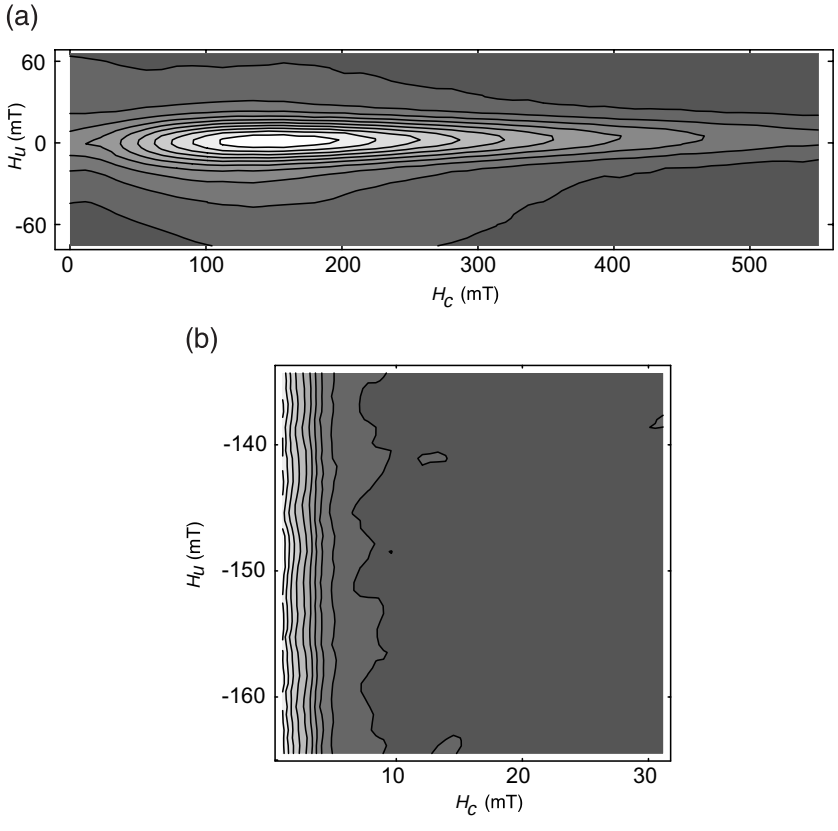

Figure 3. (a) FORC diagram for the synthetic haematite sample ($t_m = 0.7$ s). (b) High-resolution FORC diagram for the lower left-hand portion of the FORC plane for the synthetic haematite sample ($t_m = 1$ s; $SF = 3$).

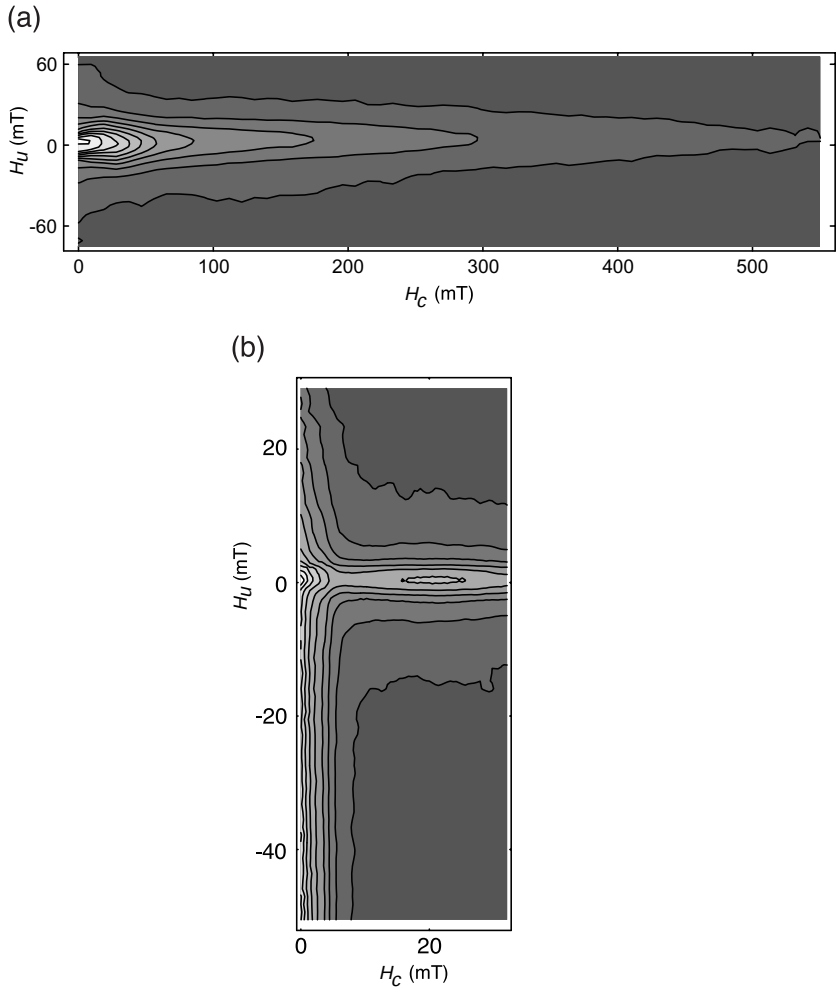

Figure 4. (a) FORC diagram for the red-bed sample 90-VAU-42 ($t_m = 0.7$ s). (b) High-resolution FORC diagram for the lower left-hand portion of the FORC plane for the red-bed sample ($t_m = 1$ s; $SF = 3$).

Chantrell 1992)

$$\Delta E \left\{ \begin{matrix} \uparrow\downarrow \\ \downarrow\uparrow \end{matrix} \right\} = \frac{\mu_o V M_s H_k}{2} \left(1 \pm \frac{H}{H_k}\right)^2, \quad \text{with } -H_k < H < H_k, \tag{2}$$

and where the moment will have a negative orientation for $H < -H_k$, and a positive orientation for $H > H_k$.

The Néel–Arrhenius law states that the magnetic moment of a ferromagnetic single-domain particle will pass over an energy barrier ΔE at the rate $f_o \exp[-\Delta E/(k_B T)]$, where k_B is the Boltzmann constant, T is the absolute temperature and f_o (sometimes referred to as an attempt frequency) is estimated to lie between 10^8 and 10^{13} (Xiao *et al.* 1986; Moskowitz *et al.* 1997). Let us introduce the dimensionless applied field $h \equiv H/H_k$ and $\Gamma(h) \equiv \exp[-\mu_o V M_s H_k (1+h)^2/2k_B T]$. For $-1 < h < 1$, the rate of change of M will be

$$\begin{aligned} \dot{M} &= -(1+M) f_o \Gamma[h] + (1-M) f_o \Gamma[-h] \\ &= f_o(-M\{\Gamma[h] + \Gamma[-h]\} + \{\Gamma[-h] - \Gamma[h]\}). \end{aligned} \tag{3}$$

With an initial magnetization M_o, eq. (3) has the solution

$$\begin{aligned} M(t) = M_o &\exp(-f_o t\{\Gamma[h] - \Gamma[-h]\}) \\ &+ [1 - \exp(-f_o t\{\Gamma[h] - \Gamma[-h]\})] \left[\frac{\Gamma[-h] - \Gamma[h]}{\Gamma[h] + \Gamma[-h]}\right]. \end{aligned} \tag{4}$$

Let us next index the points in a set of FORC data by $\{i, j\}$, where i denotes the position of a FORC within a set of FORCs, and j denotes the position of a data point on an individual FORC, and where $\{i, j = 1\}$ is the reversal point on the ith FORC. Let $h_{i,j}$ and $M_{i,j}$ denote the applied field and magnetization at the $\{i, j\}$ data point. We then have $h_{i,j} = h_{1,1} + [(i-1) - (j-1)]FS$, where FS is the field step between successive measurements. FS and $h_{1,1}$ now determine the entire data set.

In the following model, the system will spend a time t_m at each point on a FORC, where t_m is the measurement time. The magnetization at the end of this time will be taken as the magnetization at the corresponding data point. We will treat the applied field as if it instantaneously jumps from one field value to the next on a FORC. However, we need to consider explicitly that some amount of time is necessary to ramp the

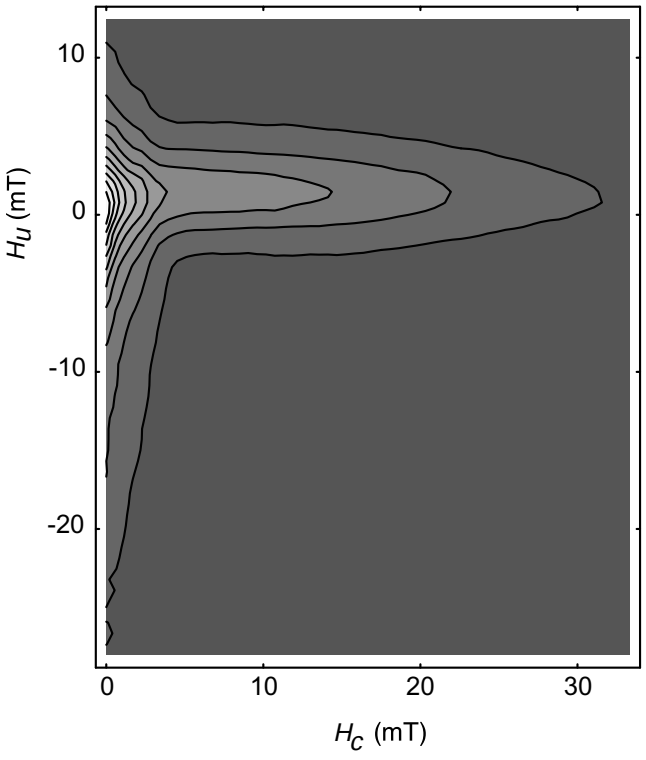

Figure 5. FORC diagram for sample CS914 ($t_m = 0.3$ s; $SF = 3$).

applied field down from positive saturation and to stop at a reversal field. Let us treat this process as if the applied field jumps instantaneously from positive saturation to the reversal field and then spends some time t_{re} at the reversal field before the first measurement begins. We can denote the measurement time as $t^m_{i,j} = t_m + t_{re}\delta_{j,1}$, where $\delta_{j,1} = 1$ for $j = 1$ and 0 for $j \neq 1$. Based on direct observations of our magnetometer, t_{re} should be roughly 2 s. Modelled in this way, $M_{i,j}$ becomes

$$M_{i,j} = 1 \qquad \text{for } 1 < h_{i,j},$$

$$M_{i,j} = -1 \qquad \text{for } h_{i,j} < -1,$$

and for $-1 < h_{i,j} < 1$,

$$\begin{aligned} M_{i,j} = {} & M_{i,j-1}\exp[-t^m_{i,j} f_o\{\Gamma[h_{i,j}] - \Gamma[-h_{i,j}]\}] \\ & + (1 - \exp[-t^m_{i,j} f_o\{\Gamma[h_{i,j}] - \Gamma[-h_{i,j}]\}]) \\ & \times \left(\frac{\Gamma[-h_{i,j}] - \Gamma[h_{i,j}]}{\Gamma[h_{i,j}] + \Gamma[-h_{i,j}]}\right), \end{aligned} \tag{5}$$

where $M_{i,0} = 1$ is the initial magnetization at the instant the applied field jumps from positive saturation to the reversal point on the ith FORC.

(ii) Distributed H_k and V

Next let us consider a distribution of anisotropy fields with a peak at $\bar{H}_k$ and a distribution of volumes with a peak at $\bar{V}$. Let us define a dimensionless anisotropy field $h_k \equiv H/\bar{H}_k$ and a dimensionless distribution $g(h_k)$, which has a peak at 1 and where $\int_0^\infty dh_k g(h_k) = 1$. A log-normal distribution is often used for $g(h_k)$,

$$g(h_k) = \exp(-\log[h_k \exp(-\sigma_h^2)]^2/2\sigma_h^2)/(\sigma_h h_k \sqrt{2\pi}), \tag{6}$$

where σ_h is the log-normal standard deviation. Similarly, let us define $v \equiv V/\bar{V}$, a log-normal distribution of particle volumes $f(v)$, and σ_v. Let us introduce a dimensionless temperature $\bar{T} \equiv 2k_B T/(\mu_o M_s \bar{H}_k \bar{V})$ and the notation $\Gamma(h_k, v, h) \equiv \exp[-vh_k(1 + h/h_k)^2/\bar{T}]$, where $h \equiv H/\bar{H}_k$. The total magnetic moment is

$$M_{i,j} = \int_0^\infty dv f(v) \int_0^\infty dh_k g(h_k) M_{i,j}(h_k, v), \tag{7}$$

where

$$M_{i,j}(h_k, v) = 1 \qquad \text{for } h_k < h_{i,j},$$

$$M_{i,j}(h_k, v) = -1 \qquad \text{for } h_{i,j} < -h_k,$$

and for $-h_{i,j} < h_k < h_{i,j}$,

$$\begin{aligned} M_{i,j}(h_k, v) = {} & M_{i,j-1}(h_k, v) \\ & \times \exp[-f_o t^m_{i,j}\{\Gamma[h_k, v, h_{i,j}] - \Gamma[h_k, v, -h_{i,j}]\}] \\ & + (1 - \exp[-f_o t^m_{i,j}(\Gamma[h_k, v, h_{i,j}] - \Gamma[h_k, v, -h_{i,j}])]) \\ & \times \left(\frac{\Gamma[h_k, v, -h_{i,j}] - \Gamma[h_i v, h_{i,j}]}{\Gamma[h_k, v, h_{i,j}] + \Gamma[h_k, v, -h_{i,j}]}\right) \end{aligned} \tag{8}$$

and $M_{i,0}(h_k, v) = 1$. This model of an assemblage of non-interacting, uniaxially anisotropic single-domain particles was used to calculate the FORC distributions shown in Figs 6–8 (see Discussion below).

(iii) Calculations

For the FORC diagrams in Figs 6 and 7, we used model parameters that most accurately represent our synthetic haematite sample: $t_m = 0.7$ s, $t_{re} = 2$ s, $\sigma_h = 0.225$, $\bar{H}_k = 400$ mT, $f_o = 2 \times 10^9$ s^{-1}. We found good agreement when the particles were assumed to have nearly uniform volumes, so we let $\sigma_v = 0$. FORC diagrams were calculated for this model with increasing values of $\bar{T}$ (Figs 6 and 7). At $\bar{T} = 0.00779$, the model gives an excellent fit between the calculated FORC diagram (Fig. 6b) and the FORC diagram for the synthetic haematite sample (Fig. 3a). The contours on the FORC diagram in Fig. 3(a) have some degree of vertical spread, which can be attributed to interactions. If this vertical spread is ignored, then agreement between Fig. 3(a) and Fig. 6(b) is good. At $\bar{T} = 0.01243$, the model produces significant vertical contours in the lower quadrant of a higher-resolution FORC diagram (Fig. 7), which agrees well with the higher-resolution FORC diagram for the red-bed sample (Fig. 4b).

In the calculation of Fig. 8, we let $\sigma_v = 0.39$, $f_o = 10^8$ s^{-1}, $t_m = 1$ s, $t_{re} = 1$ s, $\sigma_h = 0.19$, $\bar{T} = 0.10645$, and $\bar{H}_k = 55.6$ mT. For this calculation, we used a power of (3/2) instead of 2 in eq. (2), as suggested by Victora (1989). The resulting FORC diagram (Fig. 8) compares well with that for sample CS914 (Fig. 5).

DISCUSSION

The results from our numerical model of non-interacting, uniaxially anisotropic, single-domain particles exhibit several manifestations of thermal relaxation. First, increasing $\bar{T}$ shifts the distribution peak towards reduced coercivity values on a FORC diagram (Fig. 6). The fact that some of the contours

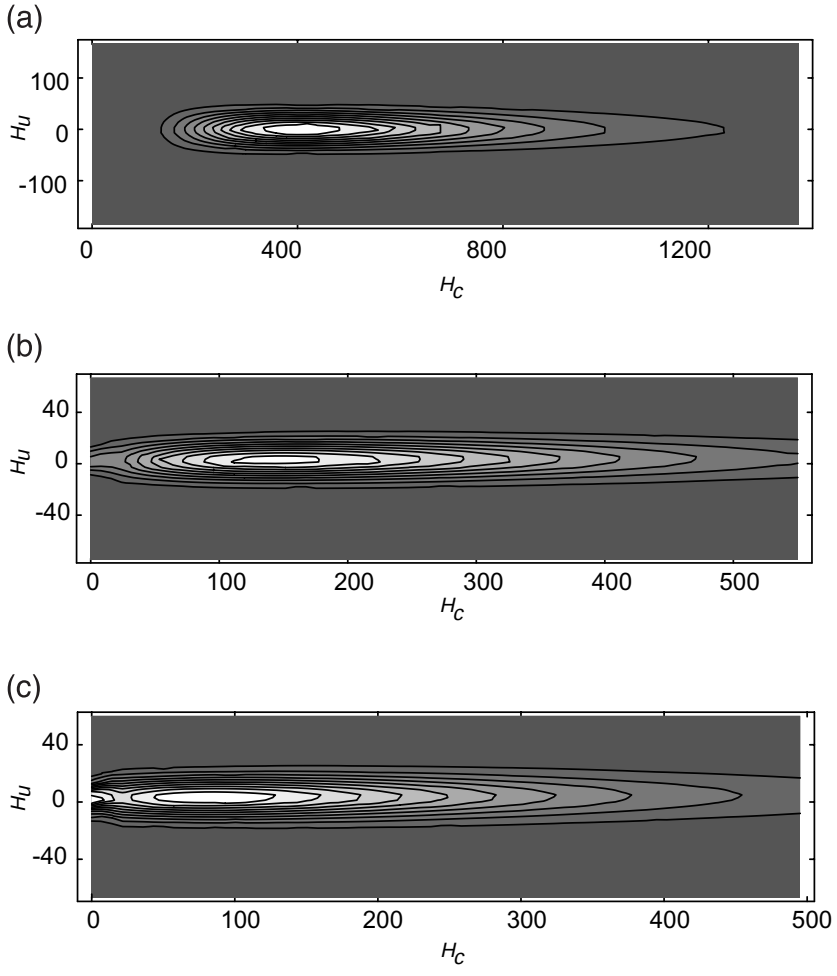

Figure 6. FORC diagrams produced using results from our numerical model for (a) $\bar{T}=0$, (b) $\bar{T}=0.00779$ and (c) $\bar{T}=0.01213$. The model parameters are uniform volume (i.e. $v=1$), $t_m=0.7$ s, $t_{re}=2$ s, $\ln(\sigma_h)=0.225$, $\bar{H}_k=180.2$ mT, $f_o=2\times10^9$ s^{-1} and $SF=3$.

in Figs 6(b) and (c) intersect the $H_c=0$ axis indicates that a fraction of the FORC distribution is effectively 'pushed' off the FORC diagram: this implies the presence of SP material.

A second manifestation of thermal relaxation at intermediate temperatures is the presence of a secondary peak about the origin of a FORC diagram in addition to the primary single-domain FORC distribution peak (Figs 1d, 4b and 6c). Upon first inspection, this secondary peak seems to imply a bimodal distribution of either the particle volumes or anisotropies. However, our calculations demonstrate that this is not necessarily the case. Rather, such secondary peaks, which are centred about the origin of the FORC diagram, can be due to SP particles that have undergone thermal relaxation in a system with unimodal volume and anisotropy distributions (Fig. 6c).

The results in Fig. 8 indicate that at high enough $\bar{T}$, the main single-domain distribution peak will disappear entirely, leaving only the peak about the origin of the FORC diagram due to SP material. We can therefore conclude from Fig. 5 that sample CS914 is magnetically dominated by SP material [which is consistent with the findings of Worm (1998, 1999) and Worm & Jackson (1999)]. By similar reasoning, our red-bed sample must also contain a significant fraction of SP material (Fig. 4).

The third manifestation of thermal relaxation is an upward shift of the FORC distribution above the $H_u=0$ axis (Figs 4b, 5, 6, 7 and 8). A qualitative explanation for this shift is as follows: due to the fact that an applied field cannot be changed instantaneously, a magnetometer will always have an effective pause (t_{re}) at the reversal point. Combined with thermal relaxation, this produces an effective downward shift (i.e. lower field) of the reversal field, which will cause an upward shift of the FORC distribution (i.e. above the $H_u=0$ axis). To highlight this effect, let us define the function Peak$H_u(H_c)$ as the vertical (i.e. H_u) coordinate of the peak of a FORC distribution on a vertical cross-section with horizontal coordinate H_c. In Fig. 9, we plot Peak$H_u(H_c)$, calculated from the FORC distribution in Fig. 6(b), as a function of H_c. A positive (upward) shift of the distribution occurs at all values of H_c, and the magnitude of this shift is a function of H_c.

Peak$H_u(H_c)$ was also calculated from the FORC distribution in Fig. 3(a) for the synthetic haematite sample. The situation here is more complicated because, as shown in a previous paper, interactions in fine magnetic particle systems cause a downward shift of the FORC distribution (Pike *et al.* 1999). The interactions in the synthetic haematite sample are weak, but strong enough to cause a slight downward shift in the FORC distribution. Hence, Peak$H_u(H_c)$ calculated from Fig. 3(a) results from the superposition of a downward shift due to interactions and an upward shift due to thermal relaxation. However, at large H_c, the shift due to interactions vanishes (Pike *et al.* 1999) leaving only the shift due to thermal relaxation. Hence, at large

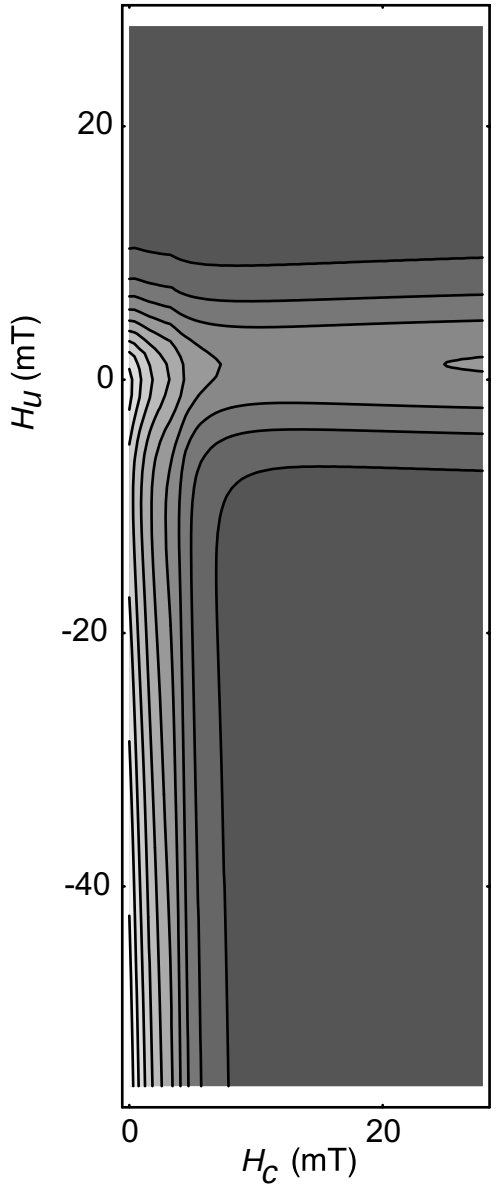

Figure 7. High-resolution FORC diagram produced using the same parameters as in Fig. 6 but at $\bar{T}=0.01243$ ($SF=3$).

H_c there should be agreement between Peak$H_u(H_c)$ of our model (which does not include interactions) and that of the synthetic haematite sample, as observed in Fig. 9.

A fourth manifestation of thermal relaxation is the presence of vertical contours near the vertical axis in the lower quadrant of a FORC diagram. These vertical contours are observed in calculations (Fig. 7) and in experimental results (Figs 3b and 4b). To give an intuitive idea of how they arise, consider a system of non-interacting single-domain particles, and let us assume, for the sake of simplification, that there is no reversible component of magnetization. In the absence of thermal relaxation, after the applied field has reached the reversal point there is no further decrease in magnetization during measurement of the FORCs (Fig. 10a), and the FORCs will have zero slope until positive fields are reached. On the other hand, in the presence of thermal relaxation, the FORCs will relax slightly in a negative direction even when the applied

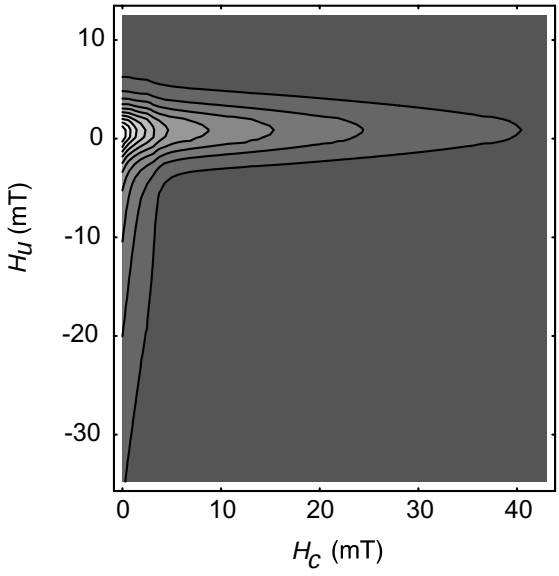

Figure 8. FORC diagram produced using results from our numerical model with the following parameters: $\sigma_v=0.39$, $f_o=10^8$ s^{-1}, $t_m=1$ s, $t_{re}=1$ s, $\sigma_h=0.19$, $\bar{T}=0.10645$, $\bar{H}_k=57.6$ mT and $SF=3$.

field is increasing (Fig. 10b). It can be shown that on a FORC diagram the relaxation seen in Fig. 10(b) will produce vertical contours in the lower quadrant such as those shown in Figs 3(b) and 4(b). Some thermal relaxation would be expected in any magnetic particle assemblage, which would imply that these vertical contours would be present on any FORC diagram. However, in many samples this effect is too weak to be observed on a normal-resolution FORC diagram (e.g. Fig. 3a). Using higher-resolution FORC diagrams, we have observed these vertical contours in all samples containing particles close to the SP threshold volume (e.g. Fig. 3b). In contrast, vertical contours are not observable in higher-resolution FORC diagrams for magnetic recording media, which are expected to have good thermal stability.

To confirm our interpretation of the upward shift of the FORC distribution and the presence of vertical contours in the lower quadrant of FORC diagrams, we repeated some measurements with a pause of 10 s added at the reversal point of each FORC. This pause should allow the magnetizations of particles to relax before the measurement begins, rather than while the measurement is proceeding. The FORCs should therefore start at a lower level, thereby increasing the upward shift, and should be flatter near the reversal field, thereby decreasing the value of the distribution near the vertical axis in the lower quadrant. We repeated the measurement of Fig. 3(a) with a 10 s pause at each reversal point and confirmed that the resulting Peak$H_u(H_c)$ shifted significantly upwards (Fig. 9). Similarly, we repeated the measurement of Fig. 3(b) and found that the FORC distribution near the vertical axis in the lower quadrant was reduced (not shown).

When two peaks are present in a FORC diagram (e.g. Figs 1d and 4b), is it possible to determine whether the secondary peak is due to unimodal particle distributions with thermal effects or to a bimodal particle distribution with distinctly separated modes? We propose the following criterion for making this distinction. If the secondary peak is confined near the origin of the FORC diagram (see Figs 1d and 6c), then this implies unimodal particle distributions with thermal relaxation of part

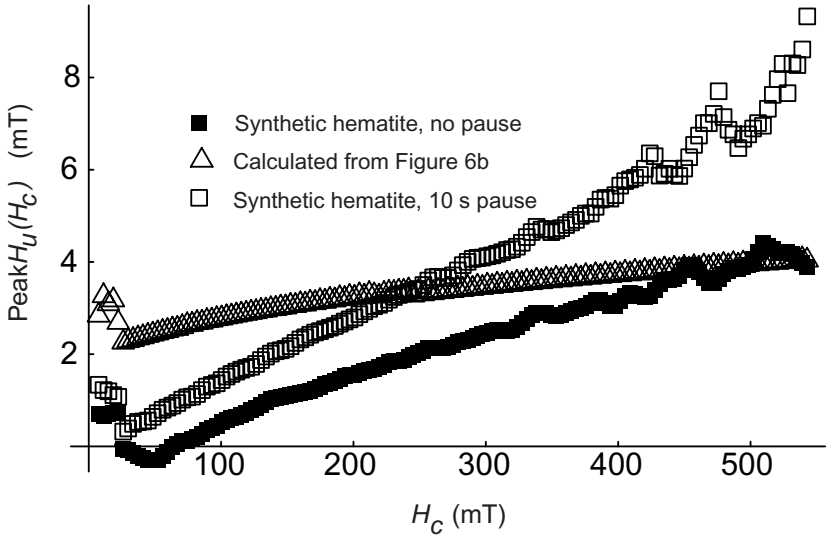

Figure 9. Peak$H_u(H_c)$ as a function of H_c for data from Fig. 3(a) (synthetic haematite sample) with and without a 10 s pause at the reversal point, and for data from Fig. 6(b) (theoretical calculation). Peak$H_u(H_c)$ is the H_u coordinate of the FORC distribution peak on a vertical cross-section passing through H_c.

of the distribution. If the secondary peak is elongated downwards into the lower quadrant, and if vertical contours appear in that quadrant (Fig. 4b), then this implies that the secondary and primary peaks arise from distinct magnetic components (i.e. bimodal particle distributions with non-overlapping modes). It is noteworthy that when the boundaries of Fig. 7, which was calculated for unimodal particle distributions, are extended to contain the primary single-domain peak, the vertical contours disappear (as was the case for Fig. 3). Thus, the presence of vertical contours is only diagnostic of bimodal particle distributions when they are observed on the same FORC diagram as a primary single-domain peak (e.g. Fig. 4b).

Finally, the slight upturn of the FORC distribution near the vertical axis in the upper quadrant (Figs 4b and 5) is a puzzling feature observed in our data. This feature is not observed in our model (Figs 7 and 8). We suggest that it results from magnetostatic interactions, and will examine this question in future work.

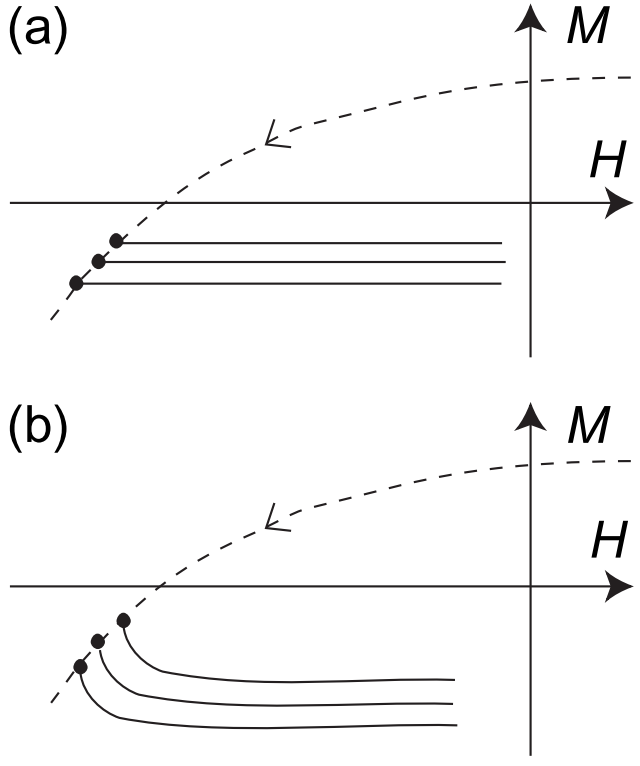

Figure 10. Schematic diagram of FORCs (a) without thermal relaxation and (b) with thermal relaxation. For the sake of illustration, the diagram is shown assuming that there is no reversible component of magnetization.

CONCLUSIONS

We have presented evidence for several manifestations of thermal relaxation on FORC diagrams. First, thermal relaxation will shift the FORC distribution to lower coercivities. Second, SP material can generate a secondary peak about the origin of the FORC diagram in addition to the primary single-domain peak. This secondary peak might, upon first inspection, appear to indicate a bimodal distribution in particle volume or anisotropy, but this is not necessarily the case. Rather, it can result from thermal relaxation of some of the particles in an assemblage with unimodal volume or anisotropy distribution. Third, thermal relaxation will produce a small but systematic upward shift of a FORC distribution, due to the fact that an effective pause inevitably occurs at a reversal point on a FORC. Fourth, thermal relaxation can produce contours that lie near and parallel to the vertical axis in the lower quadrant of a FORC diagram. The possibility of identifying SP particles by means of these distinct features makes FORC diagrams a powerful tool for studying natural samples, particularly when the samples contain mixed magnetic particle assemblages.

ACKNOWLEDGMENTS

This work was supported by the University of Southampton Annual Grants Scheme, the Center for Statistics in Science and Technology at the University of California, Davis, and the US

National Science Foundation (EAR-9628507 and EAR-9909468). We are grateful to Horst-Ulrich Worm for supplying samples CS911 and CS914 and to Mike Jackson for a helpful and insightful review of an earlier version of the manuscript.

REFERENCES

Collinson, D.W., 1969. Investigations into the stable remanent magnetization of sediments, *Geophys. J. R. astr. Soc.,* **18,** 211–222.

Creer, K.M., 1961. Superparamagnetism in red sediments, *Geophys. J. R. astr. Soc.,* **5,** 16–28.

Dearing, J.A., Dann, R.J.L., Hay, K., Lees, J.A., Loveland, P.J., Maher, B.A. & O'Grady, K., 1996. Frequency-dependent susceptibility measurements of environmental materials, *Geophys. J. Int.,* **124,** 228–240.

Dunlop, D.J., Westcott-Lewis, M.F. & Bailey, M.E., 1990. Preisach diagrams and anhysteresis: do they measure interactions?, *Phys. Earth planet. Inter.,* **65,** 62–77.

Eick, P.M. & Schlinger, C.M., 1990. The use of magnetic susceptibility and its frequency dependence for delineation of a magnetic stratigraphy in ash-flow tuffs, *Geophys. Res. Lett.,* **17,** 783–786.

Eyre, J.K., 1997. Frequency dependence of magnetic susceptibility for populations of single-domain grains, *Geophys. J. Int.,* **129,** 209–211.

Forster, Th., Evans, M.E. & Heller, F., 1994. The frequency dependence of low field susceptibility in loess sediments, *Geophys. J. Int.,* **118,** 636–642.

Mayergoyz, I.D., 1986. Mathematical models of hysteresis, *IEEE Trans. Mag.,* **MAG-22,** 603–608.

Moskowitz, B.M., Frankel, R.B., Walton, S.A., Dickson, D.P.E., Wong, K.K.W., Douglas, T. & Mann, S., 1997. Determination of the pre-exponential frequency factor for superparamagnetic maghemite particles in magnetoferritin, *J. geophys. Res.,* **102,** 22 671–22 680.

Mullins, C.E. & Tite, M.S., 1973. Preisach diagrams and magnetic viscosity phenomena for soils and synthetic assemblies of iron oxide grains, *J. Geomag. Geoelectr.,* **25,** 213–229.

Néel, L., 1949. Théorie du trainage magnétique des ferromagnétiques en grains fin avec application aux terres cuites, *Ann. Géophys.,* **5,** 99–136.

Pfeiffer, H. & Chantrell, R.W., 1992. Calculation of the anisotropy field distribution in magnetic particle assemblies: the influence of thermal fluctuations, *J. Magn. Magn. Mater.,* **115,** 366–370.

Pike, C.R. & Fernandez, A., 1999. An investigation of magnetic reversal in submicron-scale Co dots using first order reversal curve diagrams, *J. appl. Phys.,* **85,** 6668–6676.

Pike, C.R., Roberts, A.P. & Verosub, K.L., 1999. Characterizing interactions in fine magnetic particle systems using first order reversal curves, *J. appl. Phys.,* **85,** 6660–6667.

Preisach, F., 1935. Über die magnetische Nachwirkung, *Z. Phys.,* **94,** 277–302.

Roberts, A.P., Cui, Y.L. & Verosub, K.L., 1995. Wasp-waisted hysteresis loops: mineral magnetic characteristics and discrimination of components in mixed magnetic systems, *J. geophys. Res.,* **100,** 17 909–17 924.

Roberts, A.P., Reynolds, R.L., Verosub, K.L. & Adam, D.P., 1996. Environmental magnetic implications of greigite (Fe_3S_4) formation in a 3 million year lake sediment record from Butte Valley, Northern California, *Geophys. Res. Lett.,* **23,** 2859–2862.

Roberts, A.P., Pike, C.R. & Verosub, K.L., 2000. FORC diagrams: a new tool for characterizing the magnetic properties of natural samples, *J. geophys. Res.,* **105,** 28 461–28 475.

Schlinger, C.M., Rosenbaum, J.G. & Veblen, D.R., 1988. Fe-oxide microcrystals in welded tuff from southern Nevada: origin of remanence carriers by precipitation in volcanic glass, *Geology,* **16,** 556–559.

Tauxe, L., Mullender, T.A.T. & Pick, T., 1996. Potbellies, wasp-waists, and superparamagnetism in magnetic hysteresis, *J. geophys. Res.,* **101,** 571–583.

Victora, R.H., 1989. Predicted time dependence of the switching field for magnetic materials, *Phys. Rev. Lett.,* **63,** 457–460.

Worm, H.-U., 1998. On the superparamagnetic–stable single domain transition for magnetite, and frequency dependence of susceptibility, *Geophys. J. Int.,* **133,** 201–206.

Worm, H.-U., 1999. Time-dependent IRM: a new technique for magnetic granulometry, *Geophys. Res. Lett.,* **26,** 2557–2560.

Worm, H.-U. & Jackson, M., 1999. The superparamagnetism of Yucca Mountain Tuff, *J. geophys. Res.,* **104,** 25 415–25 425.

Xiao, G., Liou, S.H., Levy, A., Taylor, J.N. & Chien, C.L., 1986. Magnetic relaxation in Fe-(SiO_2) granular films, *Phys. Rev., B,* **34,** 7573–7577.